Flux periodic magnetoconductance oscillations in GaAs/InAs core/shell nanowires

Ö. Gül,[1] N. Demarina,[2] C. Blömers,[1] T. Rieger,[1] H. Lüth,[1] M. I. Lepsa,[1] D. Grützmacher,[1] and Th. Schäpers[1,*]

[1]*Peter Grünberg Institute (PGI-9) and JARA-Fundamentals of Future Information Technology, Forschungszentrum Jülich GmbH, 52425 Jülich, Germany*

[2]*Peter Grünberg Institute (PGI-2) and JARA-Fundamentals of Future Information Technology, Forschungszentrum Jülich GmbH, 52425 Jülich, Germany*

(Received 15 October 2013; revised manuscript received 18 December 2013; published 21 January 2014)

Magnetotransport experiments on epitaxial GaAs/InAs core/shell nanowires are performed in which the InAs shell forms a tube-like conductive channel around the highly resistive GaAs core. The core/shell nanowires are grown by molecular beam epitaxy. It is found that the nanowire conductance oscillates with the magnetic field oriented parallel to its axis, with a period of the magnetic flux quantum $\phi_0 = h/e$. Related to that, it is shown that the electronic transport is mediated by closed loop quantum states encircling the wire axis rather than by electron interference of partial waves. By means of a gate voltage the conductance at zero magnetic field can be changed between an oscillation minimum and maximum. The experimental findings are supported by numerical calculations.

DOI: 10.1103/PhysRevB.89.045417 PACS number(s): 73.63.Nm, 73.23.−b

I. INTRODUCTION

The Aharonov-Bohm effect [1] is a quantum mechanical phenomenon where the wave function of a charged particle, confined in a region with no magnetic field, acquires a phase shift as a function of the enclosed flux. In fundamental research, the Aharonov-Bohm effect plays an eminent role in the study of the interaction between a charged particle and an electromagnetic potential. If the path of the interfering electron waves is predefined by an open mesoscopic ring, regular magnetoconductance oscillations can be observed [2]. In the diffusive transport these experiments can be adequately described in terms of interfering electron partial waves which propagate along classical trajectories. The resulting oscillations are periodic with the magnetic flux quantum ϕ_0, where $\phi_0 = h/e$, with h and e denoting the Planck constant and the elementary charge, respectively. The so-called Altshuler-Aronov-Spivak oscillations are observed when the electrons interfere on time-reversed paths [3,4]. In this case, the period of the conductance oscillations is $\phi_0/2$. Isolated quantum rings [5,6] based on metallic [7,8] and semiconductor [9] nanostructures have also been realized. Unlike open rings, their energy spectrum is of discrete nature consisting of closed loop states which are angular momentum states for closed circular ring structures. However, the unique electronic properties of isolated rings cannot be directly probed by transport measurements and thus, a complex metrology is often required. This phenomenon of transport through coherent closed loop states can, however, be studied in the present core/shell nanowires with contacts at both ends, which do not disturb the coherent states within the shell between both contacts.

We performed comprehensive magnetotransport experiments on epitaxial GaAs/InAs core/shell nanowires in which the InAs shell forms a tube-like conductive channel around the highly resistive GaAs core [10,11]. Using also numerical calculations, we show that in these nanoscaled semiconducting tubes, electronic transport is mediated by coherent closed-loop quantum states encircling the wire axis [12–18]. As a result, the nanowire conductance oscillates with the magnetic field oriented parallel to its axis, with a period of flux quantum ϕ_0. The observed conductance behavior is based on the flux-dependent energy spectrum of the angular momentum states in the nanowire rather than on electron interference, that is, our device is an electrically measurable, semiconductor quantum tube. Thus, in contrast to previous reports [4,19–21], our approach goes beyond the interpretation in terms of classical trajectories, and is specific to nanostructures with quantum confinement. By using InAs with its large Fermi wavelength as the conductive material and further reducing the size of the tube, we reach the limit where the transport phenomena are described on the basis of coherent states through which electrons propagate along the wire [12–16,22]. Since this limit is difficult to reach by lithographical means, we made use of self-organized epitaxially grown GaAs/InAs core/shell nanowires.

II. EXPERIMENTAL PROCEDURE

GaAs/InAs core/shell nanowires are grown by molecular beam epitaxy [10,11]. For this purpose, GaAs [111]B substrates are covered with a 6-nm-thick layer of SiO_x obtained from hydrogen silsesquioxane by thermal treatment [23]. The GaAs nanowire core is grown using a Ga-assisted growth mechanism at a substrate temperature of 590°C for 1.5 h with a Ga rate of 0.075 μm/h and an As_4 beam equivalent pressure of 10^{-6} T, corresponding to a V/III ratio of 3. After the core growth, the Ga shutter is closed and the droplet is consumed by maintaining the As flux. Subsequently, the substrate temperature is decreased to 490°C. The InAs shell is grown for 15 min with an In rate of 0.1 μm/h and the same As_4 beam equivalent pressure as used for the core. The nanowires are around 2 μm long, with a core diameter of about 100 nm and a shell thickness of 25 nm. They have a hexagonal morphology with {110} side facets and show almost no tapering. Figure 1(a) shows a scanning electron micrograph of the as-grown GaAs/InAs core/shell nanowire.

*th.schaepers@fz-juelich.de

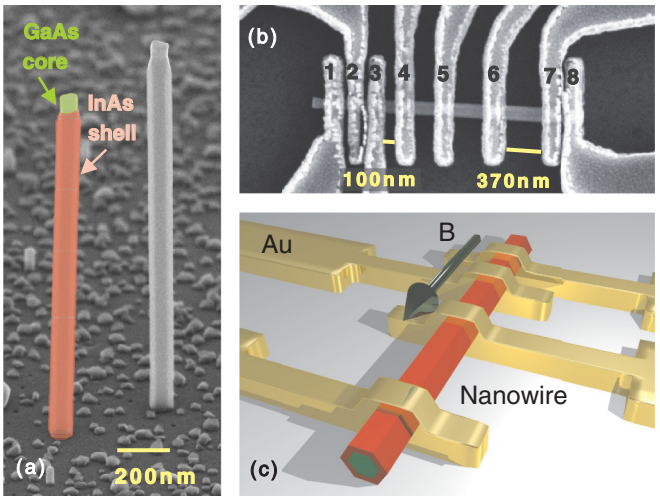

FIG. 1. (Color online) (a) Scanning electron micrograph of as-grown GaAs/InAs core/shell nanowires. The different colors in the nanowire at the left illustrate the top of the GaAs core and the InAs shell. (b) Scanning electron micrograph of the contacted GaAs/InAs core/shell nanowire. (c) Schematic of the nanowire contacting the Au electrodes. The magnetic field B is oriented parallel to the nanowire axis.

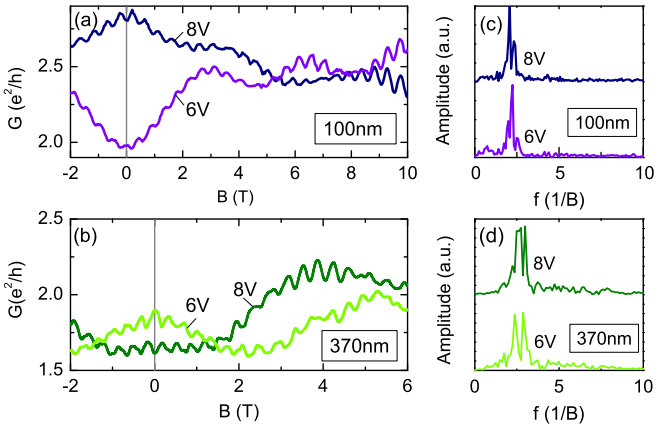

FIG. 2. (Color online) ϕ_0-periodic conductance oscillations: magnetoconductance in units of e^2/h at back-gate voltages of 6 and 8 V, respectively, for (a) the 100-nm-long and (b) the 370-nm-long nanowire segment. The peak-to-peak amplitudes of the oscillations are about 5% of the total conductance. The slowly varying background fluctuations in the magnetoconductance are attributed to universal conductance fluctuations. (c, d) The corresponding Fourier transforms. Background fluctuations in the magnetoconductance are subtracted prior to the Fourier analysis.

For transport measurements, the nanowires are separated from the growth substrate and subsequently placed on an n^+-Si[100] substrate covered with a 200-nm-thick SiO_2 insulating layer. The doped silicon substrate is used as a back gate to vary the electron density in the nanowire shell by applying a back-gate voltage V_g. To achieve low-resistance ohmic contacts between the metal electrodes and the nanowires, Ar^+ sputtering is used to remove the native oxide on the nanowire surface. Finally, each nanowire is contacted with Ti/Au electrodes. Figure 1(b) shows a scanning electron micrograph of the measured nanowire. Two segments of a single nanowire with a contact finger separation of 100 nm (between contact finger 3 and contact finger 4) and 370 nm (between contact finger 6 and contact finger 7) are measured. In addition, a second nanowire with a contact finger separation of 70 nm is investigated. All measurements are performed at a temperature of 1.8 K.

III. RESULTS AND DISCUSSION

Representative magnetoconductance curves for 100- and 370-nm-long nanowire segments are shown in Figs. 2(a) and 2(b), respectively. We observe pronounced oscillations up to 10 T, the highest magnetic field value we applied. The phase of the oscillation pattern as well as the overall conductance is modified by changing the back-gate voltage. Figures 2(c) and 2(d) show the corresponding Fourier transforms of the magnetoconductance. For the 100-nm-long segment one finds a frequency of 2.22 T^{-1}, corresponding to a period of 0.45 T, while for the 370-nm-long segment the frequency is 2.71 T^{-1}, corresponding to a smaller period of 0.37 T. Taking into account the hexagonal cross-sectional area of the nanowire $A = 3/2a^2\sqrt{3}$ with hexagon side length a, one finds that the oscillations have a period of one single flux quantum ϕ_0. The oscillations shown in Figs. 2(a) and 2(b) are superimposed on slowly varying background fluctuations. These fluctuations are attributed to universal conductance fluctuations indicating phase-coherent diffusive transport [24,25].

Figures 3(a)–3(c) show the magnetoconductance as a function of B and V_g for the 70-, 100-, and 370-nm-long segments, respectively. For all three segments clear magnetoconductance oscillations are observed over the entire gate voltage range. At zero magnetic field a locked phase of either 0 or π, corresponding to an oscillation maximum or minimum, is found. We attribute this behavior to the two-terminal nature of the transport [26–29], i.e. requirements imposed by Onsager's symmetry relations.

Fourier transforms of the magnetoconductance are calculated for all applied gate voltages. For all three nanowire segments, one finds a dominant peak structure between 2 and 2.7 T^{-1} attributed to the ϕ_0-periodic conductance oscillations, as shown in Figs. 3(d)–3(f). When the gate voltage is varied, the peak position in the Fourier spectrum slightly changes back and forth. This reflects the minor change in the oscillation period with varying gate voltage [cf. Figs. 3(a)–3(c)]. Furthermore, the variation of the gate voltage causes the intensity maximum of the ϕ_0-periodic magnetoconductance oscillations to jump between two magnetic field values characteristic of a maximum or a minimum [cf. Figs. 3(a)–3(c)].

In the following we explain the observed ϕ_0-periodic magnetoconductance oscillations and the gate-voltage-induced jumps between magnetoconductance maxima and minima consistently within the framework of electronic transport through closed loop quantum states penetrated by a magnetic flux. For calculations of the electronic states, the hexagonal cross section of the nanowire is approximated by a circle. In this case the energetic spectrum is described by using angular momentum states. The calculations are performed using a self-consistent Schrödinger-Poisson solver. The total

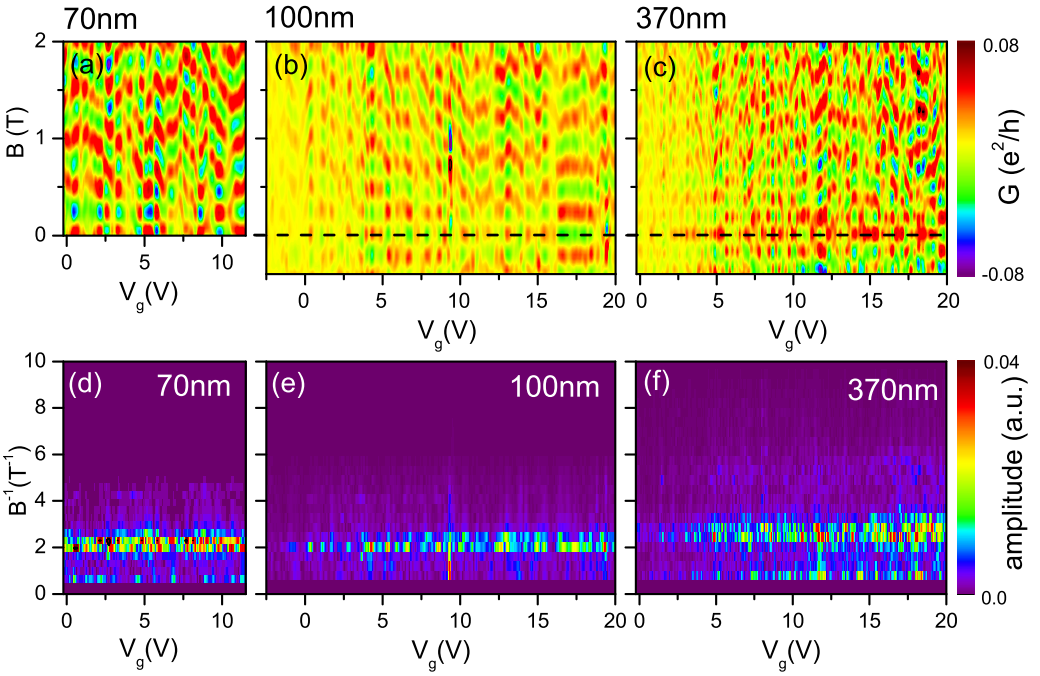

FIG. 3. (Color online) (a–c) Color plot of the magnetoconductance normalized to e^2/h as a function of the magnetic field B and gate voltage V_g for the 70-, 100-, and 370-nm-long nanowire segments, respectively, where the background conductance is subtracted. (d–f) Color plot of the amplitude of the corresponding Fourier transforms along B as a function of V_g and frequency B^{-1}.

wave function ψ is expanded as

$$\psi = \exp(ikz)\exp(il\varphi)\xi_{n,l}(r). \tag{1}$$

The first component is the plane wave with wave vector k for transport along the wire axis z, while the second one represents the angular momentum states, with the angular momentum quantum number $l = 0, \pm 1, \pm 2 \ldots$ and the azimuthal angle φ around the axis. The last term, $\xi_{n,l}(r)$, is the radial component, which depends on the radial coordinate r and describes the confinement within the InAs shell. The centrifugal force and the diamagnetic component in the Hamiltonian are expressed by the term

$$\widetilde{H}(r) = \frac{\hbar^2}{2m^* r^2}\left(-i\frac{\partial}{\partial\varphi} + \frac{\pi r^2 B}{\phi_0}\right)^2. \tag{2}$$

Because of the relatively small magnetic field considered here, we neglect the Zeeman contribution. Figure 4(a) shows the calculated conduction band profile E_c and the probability densities $|\xi_{n,l}(r)|^2$ of the first and the second sub-bands, $n = 1$ and 2, at $B = 0$. Only the first sub-band is occupied up to $l = 7$. To conserve the area of the hexagonal cross section, we consider radii of 45.5 and 68.1 nm for the core and the shell, respectively. For the GaAs core we assume a background doping of 5×10^{15} cm^{-3}. We used a constant effective electron mass of $m^* = 0.067m_e$ and $0.028m_e$ for GaAs and InAs, respectively. For the conduction band offset between GaAs and InAs we took a value of 371 meV [30], while for InAs the Fermi level E_F position at the surface with respect to the conduction band E_c was set to $E_F - E_c = 75$ meV at zero gate voltage to attain the best fit to the experimental data. In this context the essential fitting parameter is the electron concentration of the InAs shell. It was determined to 1×10^{12} cm^{-2} from field-effect transistor measurements. Because of charging effects of immobile interface states according to Hall measurements [31], the concentration of conductive electrons has been corrected to $n_{2D} = 2.5 \times 10^{11}$ cm^{-2}.

The resulting energy eigenvalue spectrum of the one-dimensional angular momentum states is shown in Fig. 4(b). The eigenvalue spectrum is periodic with the magnetic field, with a period of about 0.40 T. Due to the diamagnetic

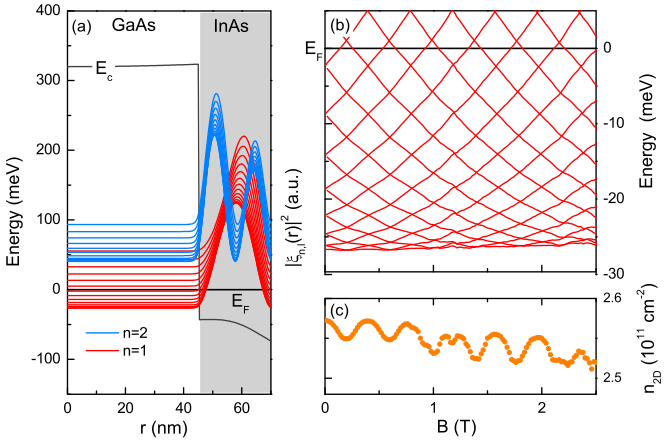

FIG. 4. (Color online) (a) Calculated conduction band profile E_c and probability density $|\xi_{n,l}(r)|^2$ for $n = 1$ and 2 at various angular momentum quantum numbers l of a GaAs/InAs core/shell nanowire with circular symmetry at $B = 0$. E_F denotes the Fermi energy. The intersection of $|\xi_{n,l}(r)|^2$ with the energy axis E at radial distance $r = 0$ reflects the energy of the eigenstates. (b) Dependence of the energy E of the states shown in (a) on the magnetic field B. (c) Electron density n_{2D} in the shell as a function of magnetic field B.

term in the Hamiltonian, the eigenvalues have a quadratical magnetic field dependence. The electron density in the shell is determined by the occupation of states with different angular momenta. Assuming a fixed position of the Fermi level at the surface due to the high density of surface/interface states at E_F, the total electron density n_{2D} oscillates with a magnetic field period of ϕ_0/A, since the energy of the levels and also the number of occupied states are periodic with ϕ_0 [cf. Fig. 4(c)]. The oscillating electron density directly contributes to the conductivity, but the detailed mathematical form depends on the type of transport.

For simplicity reasons we first consider the limiting case of ballistic transport between source and drain. In this case the Landauer-Büttiker model [32,33] requires the electronic transport to be carried out in one-dimensional channels. Each channel is defined by the quantum numbers n and l and the free motion along the z direction. In the ballistic limit without any backscattering at zero temperature, the conductance is given by $G = N \times 2e^2/h$, where N is the number of occupied spin-degenerate states located below the Fermi energy E_F. Each time the states cross E_F while B is increased, the conductance changes ideally by $2e^2/h$. At finite temperatures these abrupt conductance changes will be damped due to the broadening of the Fermi distribution function [17]. Because of the periodicity of the energy eigenvalues with ϕ_0 [cf. Fig. 3(b)], conductance variations with that period are expected. Indeed, this behavior is observed in our experiments.

In the present case, however, the observation of universal conductance fluctuations demonstrates phase-coherent quantum transport, but of a diffusive character along the wire between the two contacts, rather than ballistic transport. We imagine the transport to be mediated by the described coherent angular momentum states, but with elastic scattering processes between these states along the wire. Within this picture the ϕ_0 periodicity of the angular momentum states [cf. Fig. 4(b)] and the electron concentration as a function of the magnetic field [cf. Fig. 4(c)] is conserved. This periodic occupation of states enters the measured conductance, but in a more complex way than is described above for ballistic transport [12]. In any case, the conductance, even in the presence of elastic scattering processes along the wire, will reflect the ϕ_0 periodicity, which is observed in the experimental magnetoconductance curves shown in Figs. 2 and 3.

Depending on the strength of the disorder, scattering in the z direction may result in uncorrelated angular momentum states for different values of z, which yield a $\phi_0/2$-periodic magnetoconductance due to self-averaging [7,34,35]. In contrast, for all nanowires and gate voltage and magnetic field ranges, ϕ_0-periodic oscillation is the leading contribution, while the $\phi_0/2$-periodic oscillation amplitude is very low or not observed at all. Thus, in our system the degree of disorder is presumably small.

Nevertheless, for each one-dimensional channel the transmission coefficients will be somewhat different, depending on the scattering details. Together with the outwards shift of the $|\xi_{n,l}(r)|^2$ maximum for increasing $|l|$ [Fig. 4(a)], this may explain the slight variation of the peak position with the back-gate voltage in the Fourier spectrum shown in Figs. 3(d)–3(f). In the case of an applied back-gate voltage, the electron gas in the shell is depleted or enriched inhomogeneously around the circumference so that the eigenvalue spectrum will also depend on φ corresponding to a slight perturbation of the energy levels. However, since the back-gate voltage affects the complete wire, these perturbations will be uniform along the wire axis.

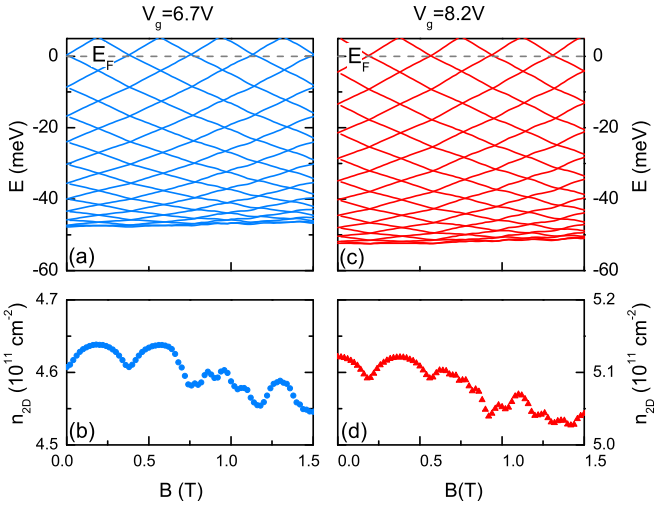

FIG. 5. (Color online) (a, b) Energy E of the angular momentum states and electron concentration n_{2D}, respectively, as functions of the magnetic field B for a gate voltage of 6.7 V, corresponding to $E_F - E_c = 115$ meV. (c, d) Respective energy of the angular momentum states and electron concentration for a gate voltage of 8.2 V, corresponding to $E_F - E_c = 124$ meV.

The present interpretation also explains the observed jumps of the magnetoconductance signal between maxima and minima upon variation of the gate voltage [Figs. 2(a), 2(b), and 3(a)–3(c)]. A gate voltage variation changes the electron concentration in the InAs shell and the Fermi level position within the shell. As the results of theoretical simulations in Fig. 5 show, reasonable gate voltage changes, from 6.7 to 8.2 V, shift the Fermi level position in the shell from $E_F - E_c = 115$ to 124 meV. According to the different crossing points of E_F with the eigenvalue parabolas shown in Figs. 5(a) and 5(c), the shell electron concentration switches from a minimum to a maximum at $B = 0$ [cf. Figs. 5(b) and 5(d)]. This is in qualitative agreement with the experiment at the same gate voltage scale. In our treatment the hexagonal cross section was approximated by a circular one. Ferrari *et al.* [14] calculated the energy levels for a zero-thickness quantum well in a hexagonal geometry. They found braids containing six levels in the energy vs magnetic field spectra. In our experiment no indications of braided levels were resolved when changing the back-gate voltage.

Using our measurement results, an ensemble averaging of the magnetoconductance can be performed over the gate voltage (ergodic hypothesis). The result of the averaging for the 370-nm-long segment is shown in Fig. 6. Close to zero magnetic field, the ϕ_0-periodic oscillations vanish, and an oscillation with a period of $\phi_0/2$ appears. This is also confirmed by the Fourier transform shown in the inset in Fig. 6. The $\phi_0/2$-periodic oscillation maximum found at $B = 0$ indicates that spin-orbit coupling contributes to the transport [4,36]. At larger magnetic fields, $B > 0.7$ T, the

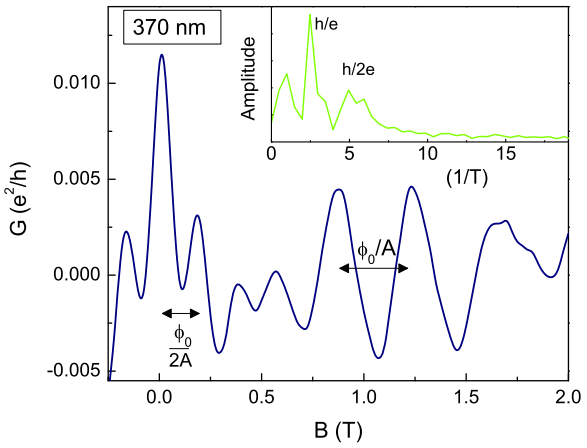

FIG. 6. (Color online) Conductance G of a nanowire with a 370-nm-long contact separation averaged over a gate voltage range from 0 to 20 V is plotted against the magnetic field B. The background conductance is subtracted. Inset: The corresponding Fourier transform. Clear peaks corresponding to ϕ_0- and $\phi_0/2$-periodic oscillations are resolved.

ϕ_0-periodic oscillations reappear because of the suppression of $\phi_0/2$-periodic oscillations due to the breaking of time-reversal symmetry [37,38]. Note that the $\phi_0/2$-periodic oscillations do not appear in the raw data. Even after an extensive averaging, the peak amplitude of the ϕ_0-periodic oscillation dominates in the Fourier spectrum (cf. Fig. 6, inset). This indicates that the system is far away from the strongly diffusive regime where energetically uncorrelated segments give rise to $\phi_0/2$-periodic magnetoconductance. The most probable reason for this is our crystalline semiconductor shell, which obviously gives rise to low scattering rates.

IV. CONCLUSIONS

One experimental highlight of this report is the realization of epitaxial GaAs/InAs core/shell nanowires which, at low temperatures, behave as quantum tubes. The ϕ_0-periodic magnetoconductance of these nanowires reveals transport through closed loop quantum states mediating the phase-coherent electron transport. This demonstrates the change in the physical basis of the ϕ_0-periodic oscillations at the transition to nanoscaled systems where coherent states govern the transport phenomena. By means of a back gate it was possible to shift the phase by π, i.e., from an oscillation maximum to a minimum, and vice versa. Our results pave the way for further experiments probing and utilizing the electronic properties of a tube on a purely quantum mechanical basis.

ACKNOWLEDGMENTS

The authors are grateful to S. Trellenkamp for electron beam writing, A. Bringer for fruitful discussions, and H. Kertz and Ch. Krause for technical assistance.

[1] Y. Aharonov and D. Bohm, Phys. Rev. **115**, 485 (1959).
[2] R. A. Webb, S. Washburn, C. P. Umbach, and R. B. Laibowitz, Phys. Rev. Lett. **54**, 2696 (1985).
[3] B. L. Al'tshuler, A. G. Aronov, and B. Z. Spivak, Pis'ma Zh. Eksp. Teo. Fiz. **33**, 101 (1981) [JETP Lett. **33**, 94 (1981)].
[4] D. Y. Sharvin and Y. V. Sharvin, Pis'ma Zh. Eksp. Teor. Fiz. **34**, 285 (1981) [JETP Lett. **34**, 272 (1981)].
[5] M. Büttiker, Y. Imry, and R. Landauer, Phys. Lett. A **96**, 365 (1983).
[6] H.-F. Cheung, Y. Gefen, E. K. Riedel, and W.-H. Shih, Phys. Rev. B **37**, 6050 (1988).
[7] L. P. Lévy, G. Dolan, J. Dunsmuir, and H. Bouchiat, Phys. Rev. Lett. **64**, 2074 (1990).
[8] V. Chandrasekhar, R. A. Webb, M. J. Brady, M. B. Ketchen, W. J. Gallagher, and A. Kleinsasser, Phys. Rev. Lett. **67**, 3578 (1991).
[9] D. Mailly, C. Chapelier, and A. Benoit, Phys. Rev. Lett. **70**, 2020 (1993).
[10] T. Rieger, M. Luysberg, Th. Schäpers, D. Grützmacher, and M. I. Lepsa, Nano Lett. **12**, 5559 (2012).
[11] C. Blömers, T. Rieger, P. Zellekens, F. Haas, M. I. Lepsa, H. Hardtdegen, O. Gül, N. Demarina, D. Grützmacher, H. Lüth *et al.*, Nanotechnology **24**, 035203 (2013).
[12] Y. Tserkovnyak and B. I. Halperin, Phys. Rev. B **74**, 245327 (2006).
[13] T. Richter, Ch. Blömers, H. Lüth, R. Calarco, M. Indlekofer, M. Marso, and Th. Schäpers, Nano Lett. **8**, 2834 (2008).
[14] G. Ferrari, G. Goldoni, A. Bertoni, G. Cuoghi, and E. Molinari, Nano Lett. **9**, 1631 (2009).
[15] S. Bellucci and P. Onorato, Physica E **41**, 1393 (2009).
[16] A. Bringer and Th. Schäpers, Phys. Rev. B **83**, 115305 (2011).
[17] G. W. Holloway, D. Shiri, C. M. Haapamaki, K. Willick, G. Watson, R. R. LaPierre, and J. Baugh, arXiv:1305.5552 [cond-mat.mes-hall].
[18] A. Manolescu, T. O. Rosdahl, S. Erlingsson, L. Serra, and V. Gudmundsson, Eur. Phys. J. B **86**, 1 (2013).
[19] A. Bachtold, C. Strunk, J.-P. Salvetat, J.-M. Bonard, L. Forro, T. Nussbaumer, and C. Schonenberger, Nature **397**, 673 (1999).
[20] M. Jung, J. S. Lee, W. Song, Y. H. Kim, S. D. Lee, N. Kim, J. Park, M.-S. Choi, S. Katsumoto, H. Lee *et al.*, Nano Lett. **8**, 3189 (2008).
[21] H. Peng, K. Lai, D. Kong, S. Meister, Y. Chen, X.-L. Qi, S.-C. Zhang, Z.-X. Shen, and Y. Cui, Nat. Mater. **9**, 225 (2010).
[22] L. Serra and M.-S. Choi, Eur. Phys. J. B **71**, 97 (2009).
[23] T. Rieger, S. Heiderich, S. Lenk, M. I. Lepsa, and D. Grützmacher, J. Cryst. Growth **353**, 39 (2012).
[24] B. Al'tshuler, Pis'ma Zh. Eksp. Teo. Fiz. **41**, 530 (1985) [JETP Lett. **41**, 648 (1985)].
[25] P. A. Lee and A. D. Stone, Phys. Rev. Lett. **55**, 1622, (1985).
[26] A. Levy Yeyati and M. Büttiker, Phys. Rev. B **52**, R14360 (1995).
[27] G. Cernicchiaro, T. Martin, K. Hasselbach, D. Mailly, and A. Benoit, Phys. Rev. Lett. **79**, 273 (1997).
[28] S. Pedersen, A. E. Hansen, A. Kristensen, C. B. Sørensen, and P. E. Lindelof, Phys. Rev. B **61**, 5457 (2000).

[29] S. S. Buchholz, S. F. Fischer, U. Kunze, M. Bell, D. Reuter, and A. D. Wieck, Phys. Rev. B **82**, 045432 (2010).
[30] M.-E. Pistol and C. E. Pryor, Phys. Rev. B **78**, 115319 (2008).
[31] C. Blömers, T. Grap, M. I. Lepsa, J. Moers, S. Trellenkamp, D. Grützmacher, H. Lüth, and Th. Schäpers, Appl. Phys. Lett. **101**, 152106 (2012).
[32] R. Landauer, IBM J. Res. Dev. **1**, 223 (1957).
[33] M. Büttiker, Phys. Rev. Lett. **57**, 1761 (1986).
[34] J. P. Carini, K. A. Muttalib, and S. R. Nagel, Phys. Rev. Lett. **53**, 102 (1984).
[35] G. Montambaux, H. Bouchiat, D. Sigeti, and R. Friesner, Phys. Rev. B **42**, 7647 (1990).
[36] J. Nitta and T. Bergsten, New J. Phys. **9**, 341 (2007).
[37] A. D. Stone and Y. Imry, Phys. Rev. Lett. **56**, 189 (1986).
[38] C. P. Umbach, C. Van Haesendonck, R. B. Laibowitz, S. Washburn, and R. A. Webb, Phys. Rev. Lett. **56**, 386 (1986).